

# Subgrid modeling of the filtered equation of state with application to real-fluid turbulent mixing at supercritical pressures

Cite as: Phys. Fluids **34**, 065112 (2022); <https://doi.org/10.1063/5.0088074>

Submitted: 12 February 2022 • Accepted: 09 May 2022 • Published Online: 02 June 2022

 Umesh Unnikrishnan, Joseph C. Oefelein and  Vigor Yang



[View Online](#)



[Export Citation](#)



[CrossMark](#)



APL Machine Learning

Open, quality research for the networking communities

MEET OUR NEW EDITOR-IN-CHIEF

[LEARN MORE](#)

# Subgrid modeling of the filtered equation of state with application to real-fluid turbulent mixing at supercritical pressures

Cite as: Phys. Fluids **34**, 065112 (2022); doi: [10.1063/5.0088074](https://doi.org/10.1063/5.0088074)

Submitted: 12 February 2022 · Accepted: 9 May 2022 ·

Published Online: 2 June 2022



View Online



Export Citation



CrossMark

Umesh Unnikrishnan,<sup>1,a)</sup>  Joseph C. Oefelein,<sup>1,b)</sup> and Vigor Yang<sup>1,2,c)</sup> 

## AFFILIATIONS

<sup>1</sup>School of Aerospace Engineering, Georgia Institute of Technology, Atlanta, Georgia 30332, USA

<sup>2</sup>Ralph N. Read Chair and Regents Professor, School of Aerospace Engineering, Georgia Institute of Technology, Atlanta, Georgia 30332, USA

**Note:** This paper is part of the special topic, Development and Validation of Models for Turbulent Reacting Flows.

<sup>a)</sup>[umesh.aero@gatech.edu](mailto:umesh.aero@gatech.edu)

<sup>b)</sup>[joseph.oefelein@aerospace.gatech.edu](mailto:joseph.oefelein@aerospace.gatech.edu)

<sup>c)</sup>Author to whom correspondence should be addressed: [vigor.yang@aerospace.gatech.edu](mailto:vigor.yang@aerospace.gatech.edu)

## ABSTRACT

Simulation of turbulent mixing and combustion at supercritical pressures requires the use of a real-fluid equation of state (EOS) to represent the nonideal, nonlinear thermodynamic behavior of fluids under these conditions. The simplified representation of the filtered EOS in the large eddy simulation methodology introduces inconsistencies in the computed filtered thermodynamic state. This study investigates these inconsistencies and novel subgrid modeling approaches to address these issues, using high-resolution direct numerical simulation of a transcritical mixing layer. Errors incurred by not accounting for subgrid effects in the EOS are quantified, and fundamental insights are drawn regarding the nature of these effects. Then, different modeling approaches are proposed and investigated to obtain a more accurate representation of the filtered EOS. The evaluation of the filtered EOS in terms of the Reynolds-filtered state variables is considered instead of the conventional Favre-filtered variables. A dynamic gradient model is formulated by building upon the ideas of dynamic modeling to render a functional form for the subgrid EOS expressed in terms of the resolved flow gradients. A scale-similarity model formulation for the subgrid EOS is also constructed and examined. Finally, a model for the filtered EOS is derived using a presumed filtered density function that accounts for the effect of subgrid-scale fluctuations. The performance of each model is evaluated using various metrics, and the relative accuracy of each modeling approach is compared and contrasted at different filter sizes.

Published under an exclusive license by AIP Publishing. <https://doi.org/10.1063/5.0088074>

## I. INTRODUCTION

A detailed understanding of turbulent mixing in combustion devices is a prerequisite for the design of efficient and stable propulsion systems. The complexity of the problem is primarily due to the wide range of length and timescales associated with high Reynolds number flows and the highly nonlinear coupling of flow processes occurring at these different scales. Computational fluid dynamics has enabled detailed descriptions of the intricacies of turbulent flows. Among the different approaches for modeling turbulence, large eddy simulation (LES) is a powerful tool that offers a viable balance between computational cost and the level of phenomenological detail represented. In LES, large-scale turbulent fluctuations, which contain most of the energy of the flow, are resolved directly on the computational

grid. The turbulent fluctuations at scales below that of the grid resolution are unresolved (referred to here as the “subgrid scales”), and the effects at these scales on the resolved scale motions are incorporated through subgrid-scale (SGS) models. With an increase in computational power over the last two decades, LES has been widely adopted by researchers for simulation of several important problems at both fundamental and engineering system levels.

An important topic of research in the advancement and application of the LES framework is the development of robust and accurate SGS models that can accurately represent the physical processes at the subgrid scales. Several studies have been dedicated to this topic.<sup>1–3</sup> The earliest model to be adopted was developed by Smagorinsky,<sup>4</sup> and the Smagorinsky model is still one of the most commonly used models.

Based on the eddy viscosity hypothesis, the subgrid-scale momentum fluxes are modeled as a turbulent stress in a form analogous to the Stokes law for viscous stresses. This assumes that the effect of the subgrid scales is to provide an energy dissipation mechanism for the large-scale fluctuations. A deficiency with the eddy viscosity hypothesis, however, is that it assumes that the subgrid-scale flux is a purely dissipative mechanism and does not allow for complex nonequilibrium turbulence phenomena such as backscatter, which have been found to exist in complex multiphysics flows.<sup>5,6</sup>

A more physical way to model SGS terms is the scale-similarity model introduced by Bardina.<sup>7</sup> The scale-similarity hypothesis approximates the energy transfer between the resolved and unresolved scales in terms of the energy transfer occurring at the smallest resolved scales. The scale similarity model achieves a high correlation to the SGS terms. Using the idea of scale similarity, Germano *et al.*<sup>8</sup> introduced a modeling approach to dynamically evaluate the Smagorinsky model coefficient in terms of the local resolved flow field. For compressible flows and flows involving multispecies transport, analogous approaches have been extended to model the SGS terms arising from the convective fluxes in the energy and species conservation equations.<sup>9,10</sup> Subgrid thermal and species mass diffusivities are computed in terms of the subgrid eddy viscosity and turbulent Prandtl and Schmidt numbers that employ either prescribed constants<sup>9,11</sup> or are computed dynamically using the Germano identity<sup>10</sup> and/or scale-similarity approach.<sup>12</sup>

Most of the subgrid-scale modeling approaches in the literature on nonreacting flows have been focused on the unclosed terms in the momentum, energy, and species transport equations. For high-pressure turbulent mixing, a key aspect of modeling is the inclusion of a nonlinear equation of state (EOS) that accounts for nonideal thermodynamic behavior. This introduces additional physical considerations for modeling the effects of subgrid-scale turbulence and its interaction with nonideal thermodynamic variations occurring at the subgrid level. These effects need to be accounted for to provide a consistent theoretical framework for LES. However, historically, LES has been developed for incompressible, nonreacting, single-component fluid flows, where the filtering of the equation of state is trivial and does not result in additional subgrid closure terms. These assumptions are not applicable in real-fluid turbulent mixing, especially in flows involving multispecies and/or thermodynamic stratifications where large variations of thermodynamic and transport properties are known to occur.<sup>13,14</sup> In such cases, filtering of small scales introduces additional SGS effects through the equation of state, which are typically neglected in current LES formulations.<sup>15–17</sup> These effects are also pertinent to the filtered ideal gas EOS under multispecies mixing and reacting conditions.<sup>18</sup>

There have been very limited investigations on the relevance of subgrid terms associated with the EOS for supercritical mixing. Selle *et al.*<sup>19</sup> investigated subgrid modeling issues using direct numerical simulation (DNS) of temporal mixing layers of different species mixtures. They found that the subgrid pressure term resulting from the filtered EOS is an important modeling consideration. They proposed a modeling approach for this term based on a Taylor series expansion, which showed moderate performance for small filter widths, but poor performance at large filter widths. Taskinoglu and Bellan<sup>20</sup> further refined this approach and conducted a *posteriori* evaluation of this model in conjunction with the other models for the SGS convective flux terms. Borghesi and Bellan<sup>21</sup> have investigated a scale-similarity approach for modeling the subgrid pressure term, which was tested as

part of a preliminary *a posteriori* study.<sup>22</sup> Using 1D laminar premixed and non-premixed flamelets, Ribert *et al.*<sup>23</sup> investigated the subgrid EOS contributions for low- and high-pressure methane flames. They reported that the subgrid terms associated with the EOS were more prominent for CH<sub>4</sub>-O<sub>2</sub> flames at high pressures where a real-fluid EOS is used. Lapenna and Creta<sup>24</sup> examined the errors in the modeling of the filtered EOS and other thermodynamic quantities using DNS of temporal mixing layers of transcritical and supercritical nitrogen jets. They explored a PDF-based closure that showed good improvement over similar studies that employed no closure for the EOS. A limitation of these works is that they considered temporal mixing layers at relatively low Reynolds numbers, which do not provide a complete description of turbulent flows under realistic conditions.

A major constraint for the investigation of turbulence modeling at realistic conditions is the prohibitive computational cost associated with three-dimensional DNS. As a result, DNS studies have often been limited to low Reynolds number flows and canonical configurations, such as temporal mixing layers. While configurations such as a three-dimensional temporal mixing layer represent some of the generic features of turbulence, they do not represent the spatiotemporal turbulence dynamics of inhomogeneous flows in practical systems. As an alternative, two-dimensional DNS offers a trade-off to reduce the computational cost while retaining more realistic flow conditions. Although 2D DNS does not fully describe the dynamics of turbulent eddies, which are inherently three-dimensional in nature, it can still provide valuable information for understanding the mathematical implications of LES filtering and the resulting subgrid terms. Model assessments using 2D DNS data have been shown to be as valuable as 3D DNS for the purpose of deriving trends for the development and assessment of subgrid models.<sup>25,26</sup>

In this study, we utilize a 2D DNS database developed in our previous work<sup>27</sup> to understand the role of subgrid turbulence effects in the filtered real-fluid EOS and to investigate modeling approaches for subgrid closure that can be applied to practical LES simulations. The DNS database is established for a spatially evolving mixing layer composed of gaseous methane and liquid oxygen at flow conditions representative of cryogenic injection and transcritical mixing of propellants in liquid rocket engines. Prior modeling approaches proposed in the literature<sup>18,28</sup> are also investigated and refined. In addition, novel modeling approaches are further explored by extending the conventional dynamic and scale-similarity modeling theories. *A priori* analyses of the proposed models are conducted to assess their performance, strengths, and limitations.

This study is organized as follows: In Sec. II, we present the mathematical formulation of the governing equations and the filtering operation to discuss the origin and relevance of the subgrid terms in the filtered EOS. In Sec. III, we briefly describe the computational framework and flow configuration used to generate the DNS data. In Sec. IV, different modeling approaches are derived, followed by an *a priori* analysis of the model performance. Finally, in Sec. V, we summarize the key findings from the study and outline directions for future work on this topic.

## II. MATHEMATICAL FORMULATION OF LES

The system of equations governing a general fluid flow is described by the conservation laws for mass, momentum, energy, and species concentrations in conjunction with appropriate constitutive

relations for the thermodynamic equation of state and other thermodynamic and transport quantities. These equations can be written as

$$\text{Mass: } \frac{\partial \rho}{\partial t} + \frac{\partial \rho u_j}{\partial x_j} = 0, \quad (1)$$

$$\text{Momentum: } \frac{\partial \rho u_i}{\partial t} + \frac{\partial}{\partial x_j} (\rho u_i u_j + p \delta_{ij}) = \frac{\partial \tau_{ij}}{\partial x_j}, \quad (2)$$

$$\text{Energy: } \frac{\partial \rho e_t}{\partial t} + \frac{\partial}{\partial x_j} ((\rho e_t + p) u_j) = \frac{\partial}{\partial x_j} (q_j + u_i \tau_{ij}), \quad (3)$$

$$\text{Species: } \frac{\partial \rho Y_k}{\partial t} + \frac{\partial \rho Y_k u_j}{\partial x_j} = \frac{\partial J_{kj}}{\partial x_j} + \dot{\omega}_k, \quad (4)$$

where  $\rho$ ,  $u_i$ ,  $p$ , and  $Y_k$  denote the density, velocity components, pressure, and mass fraction of species  $k$ , respectively. The specific total energy  $e_t$  is defined as  $e_t = e + u_i u_i / 2$ , where  $e$  is the specific internal energy.  $\dot{\omega}_k$  denotes the mass production rate of species  $k$  due to chemical reactions in a reacting system. The system of Eqs. (1)–(4) represents the governing conservation equations for DNS. The set of conserved variables solved for in this formulation is denoted as  $\mathbf{Q}_c = \{\rho, \rho u_i, \rho e_t, \rho Y_k\}$ , from which all other dependent quantities are computed. The constitutive relations for the viscous stress tensor  $\tau_{ij}$ , heat diffusive flux  $q_j$ , and species diffusive fluxes  $J_{kj}$  can be given as,

$$\tau_{ij} = \mu \left( \frac{\partial u_i}{\partial x_j} + \frac{\partial u_j}{\partial x_i} \right) - \frac{2}{3} \mu \frac{\partial u_k}{\partial x_k} \delta_{ij}, \quad (5)$$

$$q_j = -\lambda \frac{\partial T}{\partial x_j} + \sum_{k=1}^N h_k J_{kj}, \quad (6)$$

$$J_{kj} = \rho D_k \frac{\partial Y_k}{\partial x_j}. \quad (7)$$

Here, Newtonian fluid and Stokes hypothesis are assumed for the viscous stress tensor. The heat and species diffusive fluxes are assumed to follow Fourier and Fick's laws. In addition to the above equations, mathematical relations are needed for the computation of thermodynamic and transport coefficients ( $\mu$ ,  $e$ ,  $\lambda$ ,  $D_k$ , etc.). For a real fluid, these can be computed from fundamental thermodynamic theories combined with the extended principle of corresponding states<sup>29–31</sup> and high-pressure departure functions.<sup>32</sup> Details of their implementation can be found in other references.<sup>33,34</sup>

In this study, we focus on the thermodynamic equation of state, which relates the pressure, density, and temperature of a mixture with a given composition. The equation of state for a real fluid accounts for intermolecular interactions and molecular volume effects and shows significant deviation from ideal gas behavior under high-pressure conditions. A cubic equation, such as the Peng–Robinson (PR)<sup>35</sup> or Soave–Redlich–Kwong (SRK)<sup>36</sup> EOS, is often used in numerical simulations to represent these effects. Both have been shown to provide good accuracy for most conditions of practical interest.<sup>17</sup> They can be represented in a general form as

$$p = \frac{RT}{(v-b)} - \frac{a}{v^2 + uvb + wb^2}, \quad (8)$$

where  $R$  is the gas constant associated with the mixture. The parameters  $(u, w) = (2, -1)$  for the PR EOS and  $(1, 0)$  for the SRK EOS.

The coefficients  $a$  and  $b$  account for intermolecular interactions and molecular volumetric effects in the fluid. These terms are functions of the temperature and mixture composition. Here,  $v$  is the specific volume, which is the reciprocal of the density  $\rho$ .

The equation of state can be alternatively expressed in terms of the compressibility factor as

$$p = \rho ZRT. \quad (9)$$

Here, the compressibility factor  $Z$  incorporates the real-fluid effects and is computed from a cubic equation derived by substituting Eq. (9) into Eq. (8).

The computation of supercritical fluid flows is known to be susceptible to numerical instabilities stemming from spurious pressure oscillations.<sup>37</sup> To overcome this difficulty, several strategies have been investigated, including quasi-conservative schemes,<sup>38–40</sup> use of artificial dissipation,<sup>15</sup> or use of preconditioning.<sup>41,42</sup> In the preconditioning approach, a transformation is applied to the time-derivative term and the pressure is directly solved instead of the density. The preconditioning approach has been widely used and has been shown to be successful for application to flows at supercritical conditions.<sup>43–45</sup> In the preconditioned formulation, the primitive variable set  $\mathbf{Q} = \{p, u_i, T, Y_k\}$  is directly solved. This also overcomes the computational cost associated with the computation of  $T$  from  $e$  through an iterative procedure. A detailed description of the preconditioned formulation in the real-fluid framework can be found in Meng and Yang.<sup>33</sup> The equation of state is then used to evaluate the density as a function of the primitive variables as

$$\rho(\mathbf{Q}) = \frac{p}{Z(\mathbf{Q})R(\mathbf{Q})T}. \quad (10)$$

Note that  $R$  is a function of the mixture composition  $Y_k$ , and  $Z$  is a nonlinear function of the thermodynamic state  $(p, T, Y_k)$ .

In LES, a filtering operation is applied to the DNS equations to separate out the high-wavenumber (small-scale) components of the flow. The filtering operation is mathematically expressed as

$$\overline{\phi(\mathbf{x}, t)} = \iiint_V \phi(\mathbf{r}, t) G(\mathbf{x} - \mathbf{r}, t; \overline{\Delta}) d\mathbf{r}, \quad (11)$$

where  $\overline{\phi}$  is the filtered part of a field variable  $\phi$ ,  $G$  is the filter kernel, and  $V$  is the spatial volume, over which the filtering is performed. For application to compressible flows, where the density is inherently coupled with other variables in the conservative formulation, the corresponding Favre-filtered variable is defined as

$$\tilde{\phi} = \frac{\overline{\rho \phi}}{\overline{\rho}}. \quad (12)$$

The above definition implies that Favre filtering is a density-weighted filtering operation, and the resulting Favre-filtered variable  $\tilde{\phi}$  can be quite different from the filtered variable  $\overline{\phi}$  for variable density flows, particularly for those with large density stratifications or gradients present at the subgrid scales.

Applying the filtering operation and the above definitions to the DNS equations, the LES equations are obtained as follows:

$$\text{Mass } \frac{\partial \overline{\rho(\mathbf{Q})}}{\partial t} + \frac{\partial (\overline{\rho(\mathbf{Q})} \tilde{u}_j)}{\partial x_j} = 0, \quad (13)$$

$$\begin{aligned} \text{Momentum} \quad & \frac{\partial(\overline{\rho(\mathbf{Q})\tilde{u}_i})}{\partial t} + \frac{\partial}{\partial x_j}(\overline{\rho(\mathbf{Q})\tilde{u}_i\tilde{u}_j} + \overline{p}\delta_{ij}) \\ & = \frac{\partial}{\partial x_j}(\overline{\tau_{ij}(\mathbf{Q})} - \tau_{ij}^{\text{sgs}}), \end{aligned} \quad (14)$$

$$\begin{aligned} \text{Energy} \quad & \frac{\partial(\overline{\rho(\mathbf{Q})e_t(\mathbf{Q})})}{\partial t} + \frac{\partial}{\partial x_j}([\overline{\rho(\mathbf{Q})e_t(\mathbf{Q})} + \overline{p}]\tilde{u}_j) \\ & = \frac{\partial}{\partial x_j}(\overline{u_j\tau_{ij}(\mathbf{Q})} + \overline{q_j(\mathbf{Q})} - H_j^{\text{sgs}}), \end{aligned} \quad (15)$$

$$\text{Species} \quad \frac{\partial\overline{\rho(\mathbf{Q})\tilde{Y}_k}}{\partial t} + \frac{\partial(\overline{\rho(\mathbf{Q})\tilde{u}_j\tilde{Y}_k})}{\partial x_j} = \frac{\partial}{\partial x_j}(\overline{J_{kj}(\mathbf{Q})} - \Phi_{kj}^{\text{sgs}}). \quad (16)$$

The overbar and tilde denote the filtered and Favre-filtered quantities, respectively. The terms  $\tau_{ij}^{\text{sgs}}$ ,  $H_j^{\text{sgs}}$ , and  $\Phi_{kj}^{\text{sgs}}$  in Eqs. (14)–(16) represent the conventional SGS momentum, energy, and species fluxes, respectively. These terms result from simplifying the filtered convective fluxes, which involve the filtered product of two quantities (covariance) as the product of the corresponding filtered quantities. The SGS flux terms can be written as

$$\tau_{ij}^{\text{sgs}} = \overline{p}(\overline{u_i\tilde{u}_j} - \tilde{u}_i\tilde{u}_j), \quad (17)$$

$$H_j^{\text{sgs}} = \overline{p}(e_t(\mathbf{Q})\overline{u_j} - e_t(\mathbf{Q})\tilde{u}_j) + (\overline{p}u_j - \overline{p}\tilde{u}_j), \quad (18)$$

$$\Phi_{kj}^{\text{sgs}} = \overline{p}(\overline{Y_k\tilde{u}_j} - \tilde{Y}_k\tilde{u}_j). \quad (19)$$

These terms represent important interscale interactions between the resolved and subgrid-scale fields and their net effect on the dynamics of the resolved flow field. Therefore, it is important to model these terms in LES for an accurate representation of the filtered flow field and for the prediction of turbulent statistics. Several modeling approaches have been investigated for these terms for different flow configurations, and the challenges and issues are somewhat well understood for ideal gas flows at low pressures.<sup>1,2,46,47</sup>

The remaining terms in Eqs. (13)–(16) are simplified by approximating a filtered secondary quantity  $\overline{\phi(\mathbf{Q})}$  as the corresponding quantity evaluated from the filtered variables using the same functional form as in DNS, that is,  $\phi(\tilde{\mathbf{Q}})$ , where  $\tilde{\mathbf{Q}} = \{\tilde{p}, \tilde{u}_i, \tilde{T}, \tilde{Y}_k\}$  denotes the set of filtered primitive state variables that are solved in the preconditioned LES framework. The filtered quantity  $\overline{\phi(\mathbf{Q})}$  contains the effect of turbulent fluctuations of the primitive variables at all scales, while the approximated  $\phi(\tilde{\mathbf{Q}})$  only contains information on turbulent interactions at the resolved scales. Although these approximations seem to be reasonable for weakly compressible, single-species flows,<sup>12,48</sup> their validity at other flow conditions requires rigorous justification. Recent studies have shown these approximations to be inconsistent and invalid for LES of compressible, real-fluid flows, especially those involving multispecies mixing at transcritical and supercritical conditions.<sup>19,49,50</sup> The nonlinear nature of the constitutive relations and their noncommutivity with respect to the filtering operation result in additional subgrid terms that are nontrivial and require closer investigation.

In this study, we focus on the modeling of the filtered EOS, which for real-fluid flows is highly nonlinear and is an important aspect for

modeling high-pressure supercritical mixing. The filtering operation on the form of the EOS in Eq. (8) is considered as shown as follows:

$$\overline{p(\mathbf{Q}_c)} = \overline{\left( \frac{R(\mathbf{Q}_c)T}{(v(\mathbf{Q}_c) - b(\mathbf{Q}_c))} - \frac{a(\mathbf{Q}_c)}{v(\mathbf{Q}_c)^2 + uv(\mathbf{Q}_c)b(\mathbf{Q}_c) + wb(\mathbf{Q}_c)^2} \right)}.$$

For a pure substance,  $a$  is a function of temperature and  $b$  is assumed to be constant. For multicomponent mixtures,  $a$  and  $b$  are also nonlinear functions of the species composition and are obtained by applying the mixing laws to combine the corresponding coefficients of the individual components. Likewise, the molar volume is a function of the species composition and the thermodynamic state of the mixture.

Similar to the filtered convective fluxes, the equation of state also involves the filter of a combination of quantities that cannot be directly computed in LES. The nonlinear coupling among the state variables in the EOS is in fact more complex than the convective fluxes, which involve only products of two quantities. In the current LES formulations, the filtered EOS is approximated as

$$p(\overline{\mathbf{Q}_c}) = \frac{R(\overline{\mathbf{Q}_c})\tilde{T}}{(v(\overline{\mathbf{Q}_c}) - b(\overline{\mathbf{Q}_c}))} - \frac{a(\overline{\mathbf{Q}_c})}{v(\overline{\mathbf{Q}_c})^2 + uv(\overline{\mathbf{Q}_c})b(\overline{\mathbf{Q}_c}) + wb(\overline{\mathbf{Q}_c})^2}.$$

This representation is highly simplified. The quantity  $p(\overline{\mathbf{Q}_c})$  is mathematically different from  $\overline{p(\mathbf{Q}_c)}$ . Under these circumstances, neglecting the residual term becomes questionable since  $p(\overline{\mathbf{Q}_c})$  does not contain information about the interaction of scalar fields between the resolved and subgrid length scales. The effects of these processes can be nontrivial depending on the flow conditions and the level of fidelity expected in numerical simulations. For supercritical fluid flow simulations, thermodynamic processes are consequential and real-fluid effects play a significant role in the governing dynamics.<sup>51</sup> Thus, it is clearly important from a modeling perspective to accurately represent the filtered EOS in LES to accurately account for relevant subgrid thermodynamic processes.

For simplicity in representation for modeling purpose, we consider the EOS in terms of the compressibility factor as in Eq. (9). The exact filtered pressure is then given as

$$\overline{p(\mathbf{Q}_c)} = \overline{\rho Z(\mathbf{Q}_c)R(\mathbf{Q}_c)T} = \overline{\overbrace{\rho Z(\mathbf{Q}_c)R(\mathbf{Q}_c)T}},$$

and the approximated filtered pressure is given as

$$p(\overline{\mathbf{Q}_c}) = \overline{p} Z(\overline{\mathbf{Q}_c})R(\overline{\mathbf{Q}_c})T.$$

The difference between the exact and approximated filtered pressures is termed as the subgrid pressure. Selle *et al.*<sup>19</sup> investigated the subgrid pressure term for various binary species mixtures using DNS of temporal mixing layers. They quantified the magnitude of various terms in the governing equations and showed that the subgrid pressure term is comparable to the other leading terms in the momentum equation. A similar study was undertaken by Ma *et al.*<sup>49</sup> using temporal mixing layer. Ribert *et al.*<sup>23</sup> have also confirmed the relevance of this term using one-dimensional flames at high-pressure conditions. The subgrid pressure is also shown to be relevant for multispecies reacting flows under ideal gas conditions.<sup>18</sup> This term is more significant in high-pressure, nonideal

conditions,<sup>23</sup> where interscale turbulence dynamics are strongly coupled with nonlinear thermodynamics.

Similar to the pressure, in the preconditioned formulation, the EOS is used to compute density as a function of the thermodynamic state ( $p$ ,  $T$ , and  $Y_k$ ). The exact filtered density is given as

$$\overline{\rho(\mathbf{Q})} = \overline{\left(\frac{p}{Z(\mathbf{Q})R(\mathbf{Q})T}\right)}, \quad (20)$$

while the filtered density approximated in terms of filtered variables is given as

$$\rho(\tilde{\mathbf{Q}}) = \frac{\bar{p}}{Z(\tilde{\mathbf{Q}})R(\tilde{\mathbf{Q}})\bar{T}}. \quad (21)$$

The residual term, denoted as the subgrid density, can then be expressed as

$$\rho^{sgs} = \rho(\tilde{\mathbf{Q}}) - \overline{\rho(\mathbf{Q})}. \quad (22)$$

Using fully resolved data from DNS simulations, the exact filtered quantity, and, hence, the subgrid term, can be computed and investigated. This will enable us to understand the thermodynamic effects at subgrid scales and their impact on the resolved flow field, and to explore modeling strategies to account for these effects in LES simulations of real-fluid flows.

### III. APPROACH

The benchmark DNS data for investigating subgrid EOS modeling approaches were generated in a previous work.<sup>27</sup> In this section, we briefly describe the flow configuration and the computational framework used to perform the DNS simulations. Further details about the numerical setup can be found in Ref. 27.

The flow configuration studied is a planar spatially evolving mixing layer composed of gaseous methane and liquid oxygen at an operating pressure of 100 bar. A schematic of the computational domain and flow conditions is shown in Fig. 1. The two streams differ in their thermodynamic state (temperature and density) and injection velocities. The density ratio across the mixing layer is approximately 13.5, and the fuel/air momentum flux ratio is approximately 2.7. The flow parameters are representative of typical operating conditions of liquid rocket engines. The two streams are initially separated by a splitter plate with a thickness of  $\delta = 0.3$  mm, which is roughly the order of the annular thickness of LRE injectors. The Reynolds numbers of the methane and LOX streams are about  $1.6 \times 10^4$  and  $2.7 \times 10^4$ ,

respectively. A mean velocity profile following a one-seventh power law, superimposed with broadband turbulent fluctuations, is used to simulate a fully developed turbulent boundary layer at the inlet for both incoming streams. No-slip wall boundary conditions are applied on the surfaces of the splitter plate. Outflow conditions are prescribed along the top, bottom, and exit boundaries.

High-resolution 3D DNS of flows at the current Reynolds numbers is computationally demanding, especially at the selected operating conditions. Thus, as a trade-off between utility and computational cost, the DNS simulations were limited to a planar 2D configuration. Even though 2D DNS may not fully represent the dynamics of turbulence, it is useful to obtain preliminary insight and trends of LES filtering and the resulting subgrid terms.<sup>25,26</sup>

The computational domain is discretized using a grid consisting of roughly  $19 \times 10^6$  cells. The grid resolution in the transverse direction across the plate thickness is  $0.15 \mu\text{m}$ . This resolution is closely maintained across the mixing layer with some moderate stretching to account for the mixing layer growth.

The numerical framework for performing the DNS uses a finite-volume Navier–Stokes solver that has been validated and applied for a wide range of flows under similar operating conditions.<sup>44,45,52</sup> The solver uses a preconditioned formulation along with a dual-time integration. The pseudo-time integration is performed using a fourth-order Runge–Kutta scheme, while the real-time integration uses a second-order backward difference scheme. Spatial discretization of derivatives is performed using a fourth-order central difference scheme. A fourth-order matrix dissipation with a total-variation-diminishing switch<sup>53</sup> is applied to provide minimal artificial dissipation to stabilize numerical oscillations in regions with steep gradients. The modified Soave–Redlick–Kwong equation of state<sup>54</sup> is used to describe the real-fluid equation of state. The thermodynamic and transport coefficients for real-fluid mixtures are obtained using the extended principle of corresponding states and high-pressure departure functions. A detailed description of the numerical framework can be found in Meng and Yang.<sup>33</sup>

The LES grids are obtained by coarsening the DNS grid by a filter ratio  $\Delta_f$ , defined as the ratio between the local LES grid scale to the DNS grid scale ( $\Delta_f = \Delta_{LES}/\Delta_{DNS}$ ). This enables the study of modeling issues in grid topologies that are representative of LES in practical applications involving inhomogeneous flows, where nonuniform, non-isotropic grids are often employed for computational feasibility. The filtered fields are evaluated on the LES grids by applying a top-hat filter to the DNS data. It is noted that these fields are an idealization that contains information at turbulent length scales above the filtered grid size  $\Delta_{LES}$ . However, they are not the same as actual LES realizations since they are obtained by filtering the corresponding DNS fields at a particular time instant. This is in contrast to LES, which transports the filtered fields. Thus, the spatiotemporal dynamics of the large-scale motion in LES are different from that captured by *a priori* filtering of the instantaneous field from DNS. Nevertheless, the goal in SGS modeling is to obtain a modeled LES field that is as close as possible to the filtered DNS field at a given time instant. This is a prerequisite for accurately predicting the flow evolution at the resolved scales in a LES.

### IV. RESULTS AND DISCUSSION

Using the filtered fields obtained from DNS, implications and needs related to the filtered EOS can be evaluated. To accomplish this

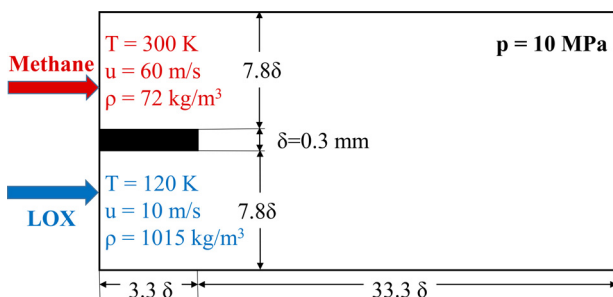


FIG. 1. Schematic of computational domain and flow configuration.<sup>27</sup>

goal, we proceed as follows. First, we perform an assessment of the errors associated with the conventional filtered EOS by analyzing the relative magnitude of the subgrid density. Second, we then evaluate the filtered EOS in terms of Reynolds-filtered quantities to contrast this with density-weighted Favre filtering. As the third, fourth, and fifth steps, we propose and perform *a priori* assessments to evaluate the accuracy of three different modeling approaches, such as the dynamic gradient model, scale similarity model, and presumed filtered-density function model. The section is concluded with detailed back-to-back assessments of how each of these models performs under identical flow conditions at different filter ratios.

### A. Relative magnitude of the subgrid density

A systematic evaluation of the terms in the filtered equations<sup>27</sup> revealed that the subgrid density term in the filtered EOS is an important modeling consideration. In the “no-model approach,” which is the currently used representation of the filtered EOS, the filtered density is directly evaluated using the filtered pressure,  $\bar{p}$  and the Favre-filtered temperature, and species mass fractions ( $\tilde{T}$ ,  $\tilde{Y}_k$ ) as shown in Eq. (21). Using the DNS data, the subgrid density defined in Eq. (22) can be computed. Figure 2 shows the spatial distribution of the subgrid density for a filter ratio  $\Delta_f = 10$ . This ratio corresponds to an LES grid that is 10 times coarser than the DNS in each direction, which is representative of typical LES simulations. The subgrid density distribution qualitatively follows the turbulent mixing layer characteristics, with the magnitude of the terms largest at the interface between the mixing layer and the LOX stream. In these regions, turbulence is generated through shear, where the gradients of the scalar fields (temperature and species mass fraction) are highest. The oxygen stream is initially at a temperature of 120 K and in a pseudo-liquid state (the critical temperature of oxygen is 154.6 K). Upon contact with the warmer gaseous methane stream, the LOX undergoes a process called pseudo-boiling<sup>55</sup> and transitions to a supercritical state. In this regime, there is a steep variation of density as a function of temperature and mixture composition. Additionally, the turbulent scalar mixing results in a locally inhomogeneous mixture with varied thermodynamic states. These two effects induce in steep density gradients at the small scales that are filtered out in LES. The subgrid density is representative of the effect of density variations at the subgrid scales on the resolved

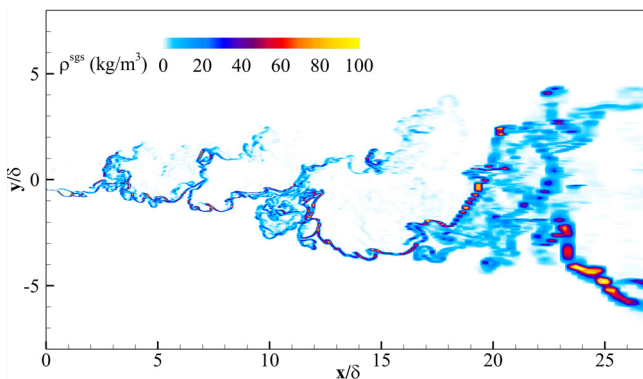


FIG. 2. Spatial distribution of the subgrid density computed from the DNS data at filter ratio  $\Delta_f = 10$ .

density. Since density (or equivalently mass) is coupled with the other transport equations, the subgrid density plays an important role in representing the underlying convective transport of momentum, energy, and species fluxes at the subgrid level.

The subgrid density is always positive for this case, implying that the approximate filtered density  $\rho(\tilde{\mathbf{Q}})$  is higher than the exact filtered density  $\overline{\rho(\mathbf{Q})}$ . Note that this is also depicted in Fig. 3(a), which shows a comparison between the exact filtered density and the modeled filtered density at filter ratio  $\Delta_f = 10$ . As described in Sec. II, the filtered secondary quantities such as shear stress, density (or pressure depending upon the EOS), and thermodynamic and transport coefficients ( $c_p$ ,  $\mu$ ,  $k$ , and  $D_{ij}$ ) are computed using Favre-filtered variables in the current LES implementations for compressible flow applications. The Favre-filtering operator is a density-weighted filtering operator, and the resulting filtered quantities are biased toward the denser species. Thus, the thermodynamic states represented by the Favre-filtered variables ( $\tilde{T}$ ,  $\tilde{Y}_k$ ) are by definition skewed toward the denser species, and the properties evaluated from these variables are thus closer to those of the denser species. In this case, the denser species is  $O_2$ , so the Favre-filtered primitive state variables ( $\tilde{T}$ ,  $\tilde{Y}_k$ ) and the modeled filtered density are biased toward those of  $O_2$ . Bias toward the denser species results in a consistent overprediction of the modeled filtered density. This will be discussed further in Sec. IV F, where Fig. 3(b) shows the distribution of relative error in the modeled filtered density as a function of the mixture fraction. The relative error is defined as the subgrid density divided by the exact filtered density. The contribution of subgrid density is low in the extremely rich and lean regions, where the effects of subgrid mixing and variation in scalar fields are minimum, and peaks in the intermediate mixture fraction regions, where the species mixing due to turbulence is in effect.

### B. Evaluation of filtered EOS in terms of Reynolds-filtered quantities (RFM)

Considering the bias associated with the Favre-filtering operator, it would be natural to evaluate the EOS in terms of non-Favre filtered variables. We term the non-Favre filtering operation in Eq. (11) as Reynolds filtering (analogous to the Reynolds-averaging operation in RANS), to make a distinction from the Favre-filtering operation. Ribert *et al.*<sup>18</sup> investigated a similar approach for computing the filtered pressure in the ideal gas EOS, by evaluating the EOS in terms of Reynolds-filtered species mass fractions instead of Favre-filtered mass fractions. The approach was proposed and analyzed for ideal, multi-component mixtures, and reasonable improvement was found. In this section, we aim to extend this approach to real-fluid, multicomponent mixtures.

It is important to note the difference in complexities between the ideal gas and real-fluid EOS; the nonlinearities in the thermodynamic behavior of individual species and the resultant mixture are different, and the filtered EOS involves covariances of three variables ( $Z$ ,  $T$ , and  $Y_k$ ) in the case of real fluids [Eq. (20)] instead of two variables ( $T$  and  $Y_k$ ) in the case of ideal gas EOS. In Ribert *et al.*,<sup>18</sup> the filtered EOS was consistently represented in terms of the Favre-filtered temperature and the Reynolds-filtered species mass fractions ( $\tilde{T}$  and  $\tilde{Y}_k$ ). However, for the real-fluid EOS, the inclusion of the compressibility factor  $Z$ , which itself is a nonlinear function of the thermodynamic state, complicates the representation of an equivalent

expression. We explore an alternate representation, designated as the Reynolds-filtered model (RFM), in which the filtered density is modeled in terms of all Reynolds-filtered primitive variables as

$$\overline{\rho(\mathbf{Q})} \approx \rho(\overline{\mathbf{Q}}), \tag{23}$$

where  $\overline{\mathbf{Q}} = (\overline{p}, \overline{u}_i, \overline{T}, \text{ and } \overline{Y}_k)$  represents the set of Reynolds-filtered primitive variables. These quantities are not usually computed in LES. Here, we compute them from the DNS data. The representation in Eq. (23) is not exact, and a subgrid term must still be included. Thus, the goal is to evaluate whether the approximation in Eq. (23) provides an improvement over the current approximation for the filtered density.

### C. Dynamic gradient model (DGM)

Following the idea of functional modeling for the subgrid fluxes such as the Smagorinsky model<sup>4</sup> or the Clark model,<sup>56</sup> we seek an analogous model for the subgrid density in terms of the gradients in the flow field. The DNS data indicate that the subgrid density is prominent in regions of strong mixing where the gradients of scalar fields are large, suggesting a possible correlation between these quantities. Based on this observation and the physical significance of this quantity as discussed in Sec. IV A, we hypothesize a model for the subgrid density as a function of the gradients of density, temperature, and species mass fraction. To evaluate this hypothesis, the correlations of the subgrid density with gradients of density, temperature, and species mass fraction are computed using the DNS data. It is found that density gradient yields the highest correlation (around 65%) with subgrid density, while temperature and species mass fraction gradients have about 39% and 30% correlations, respectively. The pressure variation in the flow field is less than 1% of the reference pressure, and the density variation corresponding to this pressure variation is negligible. The effect of the pressure gradient is not expected to significantly contribute to the subgrid term here and is not included in our modeling approach, but naturally it would need to be included for flows involving strong pressure gradients, such as shocks.

Based on the high correlation, a model form analogous to the Smagorinsky model is proposed where the subgrid density is expressed as a function of the local resolved density-gradient magnitude and the local LES filter size through a model coefficient  $C$  as

$$\rho^{sgs} = C\overline{\Delta} |\nabla\rho(\overline{\mathbf{Q}})| = C\overline{\Delta} \rho_g(\overline{\mathbf{Q}}). \tag{24}$$

Here, the notation  $\rho_g(\mathbf{Q}) = |\nabla\rho(\mathbf{Q})|$  is introduced as a shorthand to represent the magnitude of the density gradient, and  $\overline{\Delta}$  denotes the local filter (grid) scale. The model expression above can also be derived following arguments of dimensional analysis, or by filtering a Taylor series expansion of density around the LES-computed density and truncating second-order terms. Model forms including the gradients of the temperature and species mass fractions were also investigated, but the differences from the baseline model were found to be minimal.<sup>57</sup>

The model coefficient in Eq. (24) can be evaluated from the DNS data using a least-square error minimization as in linear regression analysis, by minimizing the square of the difference between the exact and modeled subgrid density. The value of  $C$  was computed using flow fields at different time instants and considering data from

different subsets of the domain that included only the core of the mixing layer, and the value was consistently found to be close to  $C \approx 21.6$ . Using this coefficient value, the model correlation with the exact value is found to be around 65%. For perspective, the Smagorinsky model has been shown to have a correlation of 20% or less for the subgrid stresses and energy fluxes, while that of the advanced dynamic model is about 60%–70%.<sup>58</sup> In sum, the proposed model for the EOS offers reasonable performance, while also being tractable in an LES simulation.

*A priori* analysis of the model performance was reported in a previous work.<sup>57</sup> Improvement in accuracy of the filtered density was achieved over the no-model approach, especially in the peak-error region near the stoichiometric mixture fraction, where the gradients and turbulent mixing are the highest. The subgrid density was, however, overpredicted in regions away from the mixing layer, where the subgrid density is negligible. This trend is attributable to the use of a globally determined model coefficient that does not consistently represent the instantaneous subgrid-scale physics in different regions of the flow field, especially in regions of low turbulent mixing. The same limitation has been recognized with the constant-coefficient Smagorinsky model in transitional and near-wall regions. Another limitation of this modeling approach lies in the generalizability of the model coefficient. Since physical reasoning cannot be presented for this value at this point, it must be assumed that the value of the coefficient for a different species mixture and different operating conditions might be different. It is speculated that the value of this coefficient might be dependent on the thermodynamic behavior of the species mixture through the EOS, but this point needs further investigation.

To overcome the limitations of the constant-coefficient model, a dynamic modeling approach for the model coefficient is applied. Using the gradient model [Eq. (24)] as a baseline, a dynamic model can be derived following Germano’s approach.<sup>8</sup> Dynamic models derived using Germano’s identity have demonstrated remarkable success over the constant-coefficient models by providing a more localized representation of subgrid-scale physics and reproducing the correct limiting behavior in different flow regions. In a dynamic model, the scale-similarity assumption is invoked to locally evaluate the model coefficient in space and time according to the local filtered flow features. The scale-similarity hypothesis assumes that the structure of turbulence and the inter-scale processes between the smallest resolved scale (grid-filter scale) and slightly larger scales (test-filter scale) are similar to those between the smallest resolved scale and the largest unresolved scale. An explicit filtering operation is applied to the LES solution at a slightly larger scale than the grid-filter width, called the test-filter scale, producing a test-filtered field. The model coefficient is then obtained by relating the subgrid term at the grid-filter (LES) and the test-filter scales, at each point in space and time.

Considering subgrid density as the unclosed term of interest,

$$\tau = \rho^{sgs} = \rho(\tilde{\mathbf{Q}}) - \overline{\rho(\mathbf{Q})} \approx C\overline{\Delta} \rho_g(\tilde{\mathbf{Q}}). \tag{25}$$

At the test-filtered level,

$$T = \rho(\widehat{\tilde{\mathbf{Q}}}) - \widehat{\overline{\rho(\mathbf{Q})}}, \tag{26}$$

where the top-hat symbol represents a filtered quantity at the test-filtered level. We then define the Leonard term as

$$\begin{aligned} \mathcal{L}_\rho &= T - \widehat{\tau} = \left( \rho(\widehat{\tilde{\rho}}) - \overline{\rho(\widehat{\tilde{\rho}})} \right) - \left( \rho(\widehat{\tilde{\rho}}) - \overline{\rho(\widehat{\tilde{\rho}})} \right) \\ &= \rho(\widehat{\tilde{\rho}}) - \overline{\rho(\widehat{\tilde{\rho}})}. \end{aligned} \tag{27}$$

This can be expressed in terms of the gradient model approximation, following the principle of scale similarity, as

$$\begin{aligned} T - \widehat{\tau} &= C\widehat{\Delta} \rho_g(\widehat{\tilde{\rho}}) - \overline{C\widehat{\Delta} \rho_g(\widehat{\tilde{\rho}})} \\ &= C\widehat{\Delta} \rho_g(\widehat{\tilde{\rho}}) - C\overline{\Delta} \rho_g(\overline{\widehat{\tilde{\rho}}}) \\ &= C\overline{\Delta} \left[ \frac{\widehat{\Delta}}{\overline{\Delta}} \rho_g(\widehat{\tilde{\rho}}) - \rho_g(\overline{\widehat{\tilde{\rho}}}) \right] = C\overline{\Delta} \mathcal{M}_\rho, \end{aligned} \tag{28}$$

where  $\mathcal{M}_\rho = \frac{\widehat{\Delta}}{\overline{\Delta}} \rho_g(\widehat{\tilde{\rho}}) - \rho_g(\overline{\widehat{\tilde{\rho}}})$ .

Each of the terms in the expressions for  $\mathcal{L}_\rho$  and  $\mathcal{M}_\rho$  can be evaluated at the test-filter level using the LES-resolved flow variables. Combining Eqs. (27) and (28) and following Lilly's least-squares approach,<sup>59</sup> the coefficient in the gradient model can be obtained as

$$C\overline{\Delta} = \frac{\langle \mathcal{L}_\rho \mathcal{M}_\rho \rangle}{\langle \mathcal{M}_\rho \mathcal{M}_\rho \rangle}. \tag{29}$$

The angular brackets indicate an averaging operation, which is usually performed to avoid unphysical oscillation of the model coefficient. In the evaluation of dynamic eddy viscosity models for the subgrid convective fluxes, a summation over the tensor or vector components, along with spatial averaging in homogeneous directions, is adopted to overcome this issue<sup>8,59</sup> whenever a homogeneous direction is present. In this case, due to the lack of homogeneity in the flow and due to the coefficient ascribed to a scalar quantity, such a procedure cannot be adopted. An alternative is to use a dynamic localization procedure<sup>60</sup> or local averaging.<sup>61</sup> In this case, we perform a local averaging over the adjacent neighboring cells, following the approach by Zang *et al.*<sup>61</sup> With the dynamic formulation, the gradient model generalizes to

$$\rho^{sgs} = \frac{\langle \mathcal{L}_\rho \mathcal{M}_\rho \rangle}{\langle \mathcal{M}_\rho \mathcal{M}_\rho \rangle} |\nabla \rho(\tilde{\rho})|. \tag{30}$$

The dynamic gradient model (DGM) formulated in Eq. (30) is parameter-free, except for the choice of the ratio between the grid- and test-filtered levels  $\widehat{\Delta}/\overline{\Delta}$ . A choice of test-filter width, which is twice the grid filter width, that is,  $\widehat{\Delta} = 2\overline{\Delta}$ , which is widely used for dynamic models for the subgrid fluxes,<sup>8,61</sup> is adopted in this study. For the *a priori* study, the test filtering is applied on the filtered LES solution, as would be performed in an LES simulation. For the test filtering, a discrete box filter is used, employing trapezoidal rule and quadratic interpolation of variables within the test-filter volume. The procedure accounts for the presence of nonuniform and nonorthogonal cells. With the modeled subgrid density, the filtered density is then evaluated from Eq. (22) as  $\overline{\rho(\tilde{\rho})} = \rho(\tilde{\rho}) - \rho^{sgs}$ .

### D. Scale-similarity model (SSM)

The principle of scale similarity was introduced by Bardina<sup>7</sup> and has been applied to directly model the subgrid stress tensor.<sup>62</sup> Cook

and Riley<sup>63</sup> have also used this principle to model the subgrid scalar variance. Following this principle, we postulate a model for the subgrid density given as

$$\rho^{sgs} \approx C_s \left( \rho(\widehat{\tilde{\rho}}) - \overline{\rho(\widehat{\tilde{\rho}})} \right), \tag{31}$$

where the quantities in the model are evaluated at the test-filter level based on the resolved variables at the LES grid level. This represents the subgrid density between the test-filter and grid-filter levels. The model coefficient  $C_s$  can be taken to be unity for the sake of simplicity, as described by Cook and Riley.<sup>63</sup> For  $C_s = 1$ , it is interesting to note that the scale-similarity model is the same as the term  $\mathcal{L}_\rho$  in the dynamic gradient model. In fact, when the density-gradient magnitudes at the grid- and test-filter scale are equal,  $\mathcal{M}_\rho$  would be equal to  $\rho_g(\tilde{\rho})$ , and the subgrid density computed with the dynamic gradient model would be equal to that computed by the scale-similarity model.

A more rigorous method is to compute the model coefficient in a dynamic manner. For this, we modify the model form such that the test filter is equal to the LES filter, similar to Bardina's model for the subgrid stress.<sup>7</sup>

$$\rho^{sgs} \approx C_{ds} \left( \rho(\tilde{\rho}) - \overline{\rho(\tilde{\rho})} \right). \tag{32}$$

Following the dynamic modeling approach, the model term  $\mathcal{M}_\rho$  can be written as

$$\mathcal{M}_\rho^s = C_{ds} \left\{ \left( \rho(\widehat{\tilde{\rho}}) - \overline{\rho(\widehat{\tilde{\rho}})} \right) - \overline{\left( \rho(\tilde{\rho}) - \overline{\rho(\tilde{\rho})} \right)} \right\},$$

and the Leonard term is as given in Eq. (27). The dynamic scale-similarity model is then formulated as

$$\rho^{sgs} = \frac{\langle \mathcal{L}_\rho \mathcal{M}_\rho^s \rangle}{\langle \mathcal{M}_\rho^s \mathcal{M}_\rho^s \rangle} \left( \rho(\tilde{\rho}) - \overline{\rho(\tilde{\rho})} \right), \tag{33}$$

where the test-filtering and spatial-averaging procedures as in the dynamic gradient model in Sec. IV C are adopted. In this study, we report the results from the scale-similarity model with  $C_s = 1$ . The dynamic scale-similarity model was also evaluated, and the differences were found to be minimal.

### E. Presumed filtered-density function (FDF) model

The filtered-density function (FDF) is an analog of the probabilistic density function (PDF) and is used in LES to represent the PDF of the subgrid-scale fluctuations.<sup>64</sup> Closure of subgrid terms using a presumed form of the FDF has been explored in several studies, including for conserved scalars in combustion problems.<sup>65,66</sup> Recently, Lapenna and Creta<sup>24</sup> investigated the application of a presumed beta PDF for the evaluation of filtered density and specific heat under transcritical and supercritical conditions. Using DNS of temporal  $N_2$  jets, they showed a good comparison of the DNS-extracted PDF to the presumed beta PDF. In their studies, they considered relatively low Reynolds number jets and a single species, with the density computed as a function of the temperature alone. In *a posteriori* studies of reacting flows,<sup>28</sup> they implemented the EOS evaluation into the flamelet model framework. The density was evaluated based on the mixture

fraction and its variance, which uniquely determine the species composition and temperature for a given value of scalar dissipation rate.

Here, we investigate the presumed FDF approach for the CH<sub>4</sub>-LOX mixing case with corrections for two discrepancies with the original approach by Lapenna and Creta.<sup>24</sup> First, with the assumption of adiabatic mixing, the relation between temperature and species composition is not linear. Moreover, the DNS data suggest that the fluctuations in temperature and species composition do not necessitate a unique mapping between the two quantities, since the governing transport processes are different. Therefore, subgrid-scale fluctuations in both scalar quantities must be individually considered for the determination of the filtered density at a given computational cell. We assume that the subgrid-scale fluctuations in the temperature and mixture fraction are statistically independent, and therefore, we can represent the joint FDF of the density as the product of the marginal FDFs with respect to the temperature and mixture fraction  $z$ . That is,  $P(T, z) = P(T)P(z)$ . We neglect the subgrid-scale fluctuations in pressure since these fluctuations are much less than 1%, and the effect of these fluctuations on the density is negligible. However, for other cases involving larger subgrid pressure fluctuations, their effect must be accounted for.

Second, we note that the presumed beta PDF form for the scalars should be attributed to the subgrid-scale Favre FDF (not the FDF) when the moments of the scalars are expressed as Favre-filtered quantities.<sup>67</sup> The Favre-filtered FDF  $\tilde{P}(\psi)$  is a density-weighted form of the FDF  $P(\psi)$  representing the density-weighted subgrid fluctuation.<sup>68</sup> The Favre FDF is used to evaluate a Favre-filtered quantity as

$$\tilde{\phi}(\psi) = \int_{-\infty}^{\infty} \phi(\psi') \tilde{P}(\psi'|\psi) d\psi'.$$

From the definition of Favre filtering [Eq. (12)], we can write  $\frac{\tilde{\rho}}{\overline{\rho}} = \frac{\tilde{\rho}}{\overline{\rho}} = 1$ . Therefore, the consistent way to evaluate the filtered density is

$$\tilde{\rho} = \frac{1}{\overline{\rho^{-1}}} = \left[ \int_0^1 \int_0^1 \frac{1}{\rho(T, z)} \tilde{P}(T, z) dT dz \right]^{-1}. \quad (34)$$

Here, the species composition is considered in terms of the mixture fraction  $z$ , which for the LOX-CH<sub>4</sub> mixing case corresponds to the mass fraction of CH<sub>4</sub>. The joint scalar Favre FDF  $\tilde{P}(T, z)$  is assumed to be the product of the marginal Favre FDFs of the two scalars. Each of the marginal Favre FDF is presumed to follow a beta PDF distribution given as

$$\tilde{P}_{beta}(\xi) = \frac{\Gamma(\alpha + \beta)}{\Gamma(\alpha)\Gamma(\beta)} \xi^{\alpha-1} (1 - \xi)^{\beta-1},$$

where the shape parameters of the PDF ( $\alpha, \beta$ ) are computed based on the Favre filtered ( $\tilde{\xi}$ ) and subgrid variance ( $\tilde{\xi}^{\prime 2}$ ) of the respective scalar fields.

$$\alpha = \tilde{\xi} \left( \frac{\tilde{\xi}}{\tilde{\xi}^{\prime 2}} - 1 \right), \quad \beta = (1 - \tilde{\xi}) \left( \frac{\tilde{\xi}}{\tilde{\xi}^{\prime 2}} - 1 \right).$$

Since the beta PDF distribution is defined over the interval [0,1], the temperature is normalized as  $\tilde{T}^* = (\tilde{T} - T_{O_2}) / (T_{CH_4} - T_{O_2})$ .

The joint Favre FDF is then given as  $\tilde{P}(\tilde{T}^*, \tilde{z}) = \tilde{P}_{beta}(\tilde{T}^*) \times \tilde{P}_{beta}(\tilde{z})$ , and the filtered density is evaluated as

$$\tilde{\rho}(\tilde{T}, \tilde{z}) = \frac{1}{\overline{\rho^{-1}}} = \left[ \int_0^1 \int_0^1 \frac{1}{\rho(T^*, z)} \tilde{P}(\tilde{T}^*, \tilde{z}) dT^* dz \right]^{-1}. \quad (35)$$

For numerical implementation, the density as a function of the scalar field ( $T^*, z$ ) is computed and stored on a grid over the interval  $(T, z) \in [T_{O_2}, T_{CH_4}] \times [0, 1]$  with  $\Delta T = 1 K$  and  $\Delta z = 0.01$ . For a *priori* analysis, the filtered and subgrid scalar variance values are directly computed from the DNS database, and the corresponding FDF and integrals are evaluated at each LES cell to compute the filtered density according to Eq. (35).

### F. A priori assessment of model performance

Figure 3 shows the comparison of the subgrid densities computed using different models at  $\Delta_f = 10$ . Note that subgrid densities are not directly computed in the Reynolds-filtered and presumed FDF models. For comparison, the subgrid densities for these cases are evaluated as the difference between the corresponding modeled filtered densities and the no-model filtered density  $\rho(\tilde{Q})$ , respectively. The subgrid densities estimated using different modeling approaches, both qualitatively and quantitatively, yield a reasonable prediction of the exact subgrid density field shown in Fig. 2. The only exception to this is the Reynolds-filtered model prediction whose estimations are nearly twice the exact value. This will be revisited again later in this section. The remaining models show a good quantitative comparison. The modeled estimates from the dynamic gradient and scale-similarity models appear to show an overall underprediction and some discrepancies in some regions, while those obtained using the presumed FDF model show a higher degree of agreement.

To quantify the effectiveness and usefulness of the proposed modeling approaches, several different metrics are considered. Figure 4(a) shows the comparison of the exact filtered densities computed from the DNS database and those evaluated using the no-model approach at filter ratio  $\Delta_f = 10$ . Figure 5 presents the corresponding comparison for the filtered densities evaluated with the modeling approaches described in Secs. IV B-IV E. Same analyses were also conducted at other filter ratios,  $\Delta_f = 5$  and 20. The results are qualitatively similar to quantitative differences in the error magnitudes in different cells. As discussed in Sec. IV A, the filtered density is overpredicted by the no-model approach, in which the density is directly computed using the Favre-filtered temperature and species mass fractions. On the other hand, the filtered density computed based on the Reynolds-filtered variables is underpredicted. The density computed using Reynolds-filtered variables does not contain information pertaining to the interaction between the primitive variables at the subgrid level and, therefore, excludes the effect of subgrid mixing on the computed density. The addition of these subgrid effects through a subgrid term might improve the prediction. For example, Ribert *et al.*<sup>18</sup> use a scale-similarity-based model to account for this term. However, we note that an analogous term could also be considered based on the Favre-filtered quantities, as in the scale-similarity model in Sec. IV D. This would also eliminate the need for an additional step to compute the Reynolds-filtered variables from the corresponding Favre-filtered

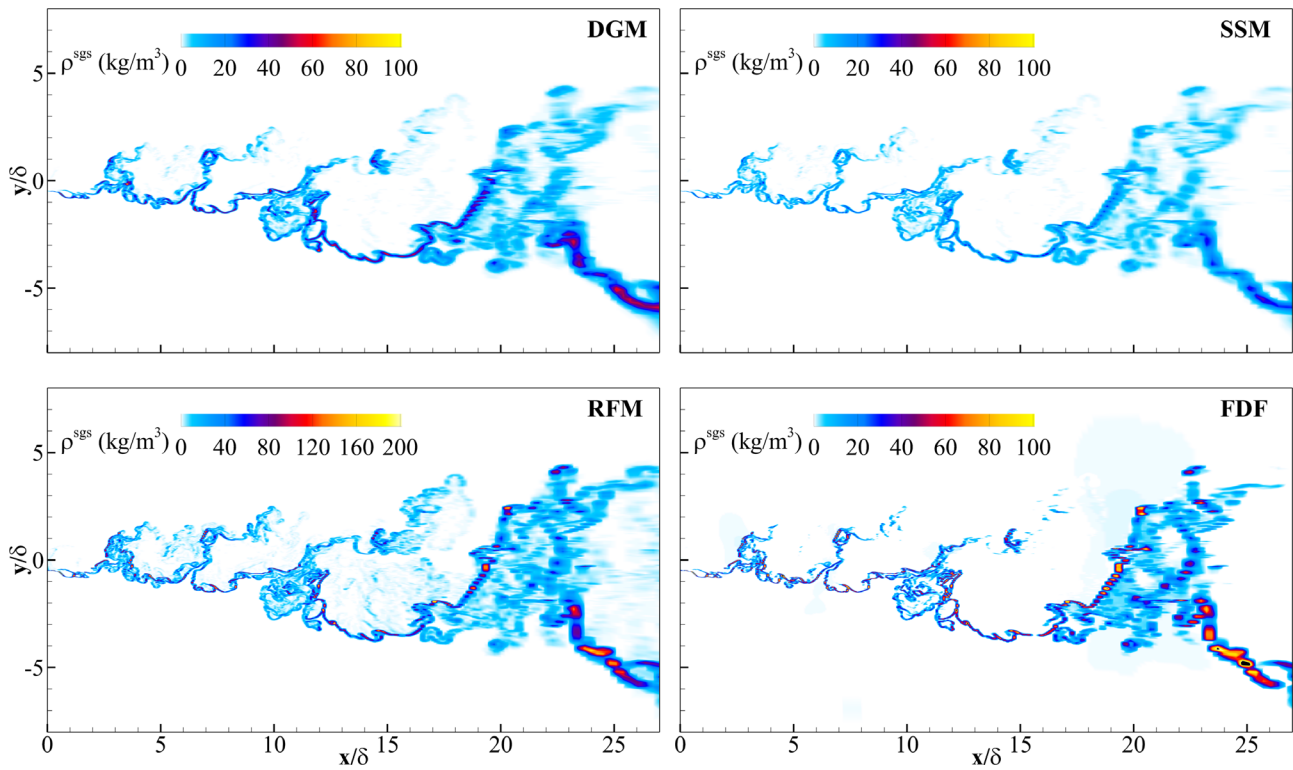


FIG. 3. Comparison of spatial distributions of the modeled subgrid densities using different modeling approaches at filter ratio  $\Delta_f = 10$ .

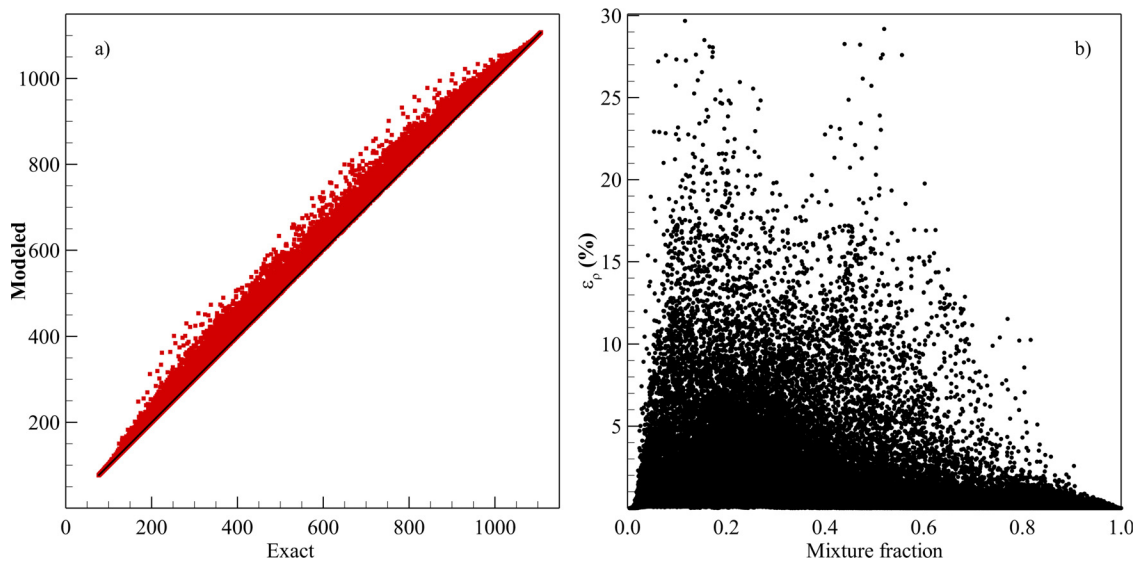


FIG. 4. (a) Comparison of DNS-filtered density (exact) with filtered density evaluated using a no-model approach and (b) distribution of relative error in computed filtered density in the mixture fraction space at filter ratio  $\Delta_f = 10$ .

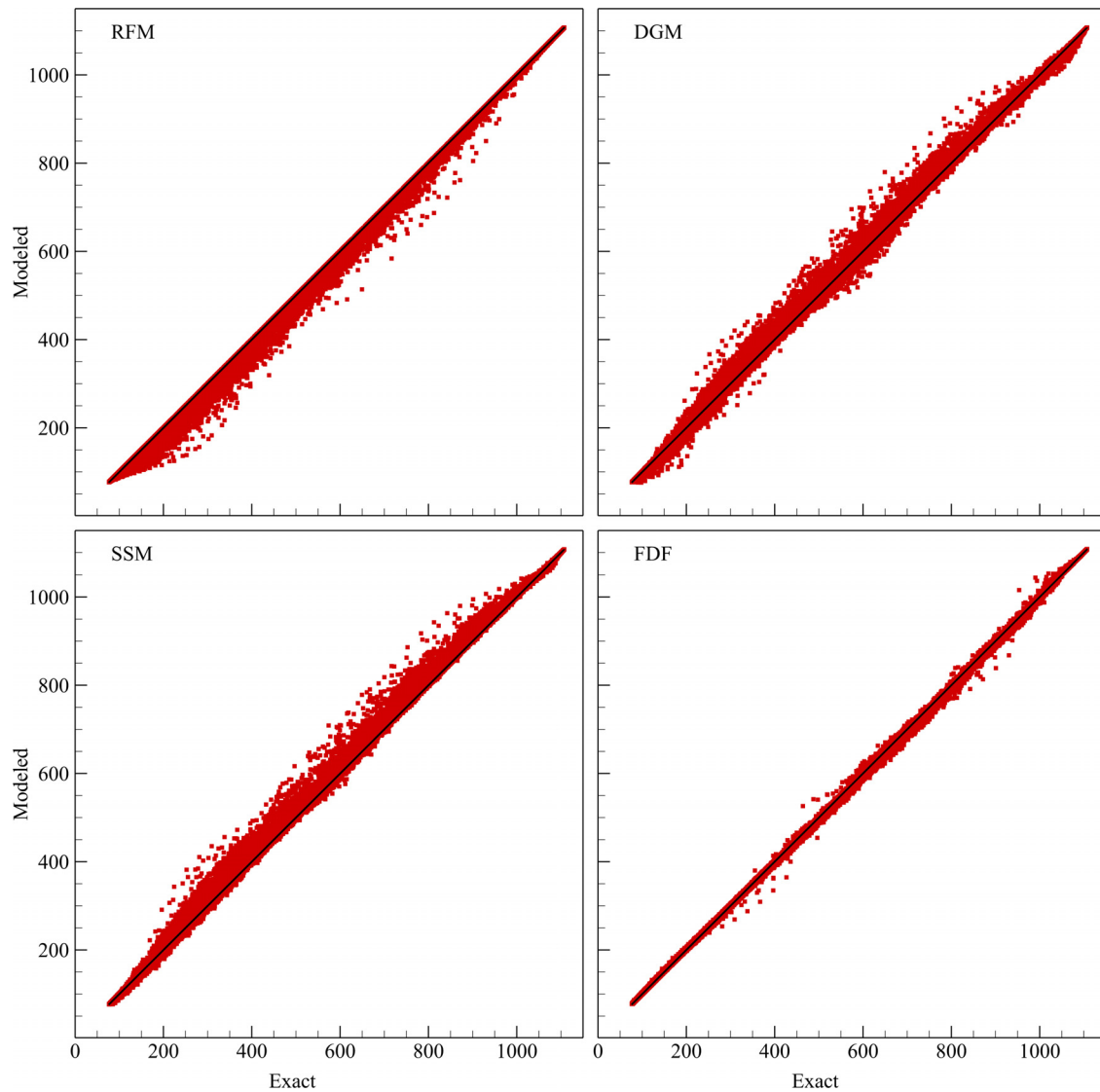


FIG. 5. Comparison of DNS-filtered density (exact) to modeled filtered density evaluated using different models at filter ratio  $\Delta_f = 10$ .

variables and would, therefore, reduce the overall computational cost of the model.

The dynamic gradient and scale-similarity models show overall improvements to the computed filtered density. The subgrid density and the filtered density evaluated with the dynamic gradient model exhibit a slight scatter in the predicted values; the scatter is worse in the absence of spatial averaging of the model coefficients. A subgrid model in principle represents the statistical effect of unresolved scales and should only be evaluated in a statistical sense. Nonstatistical evaluation of the model coefficient results in overspecification and oscillation of the value in certain regions of the flows, and statistical averaging is thus required. In this study, the local spatial averaging was confined to a three-point stencil in each spatial direction or a total of nine cells in the vicinity of an LES cell for 2D. It is possible that this averaging might not be sufficient for the filter size considered. There is also a concern

regarding the evaluation of the test filter across the transcritical interface between the two streams, which presents a sharp density gradient in the mean field. When the filter operator is applied in these regions, information on the density gradient is incorrectly interpreted as a fluctuation associated with subgrid-scale turbulence. This contribution could be more significant than realistic subgrid fluctuations, causing an inconsistency with modeling approaches, which inherently assume that all subgrid fluctuations are turbulent in nature. This subject has been broached in the context of compressible flows with shocks,<sup>69,70</sup> but it is still in the preliminary stage and the issues are not fully understood. In the present case, test filtering is found to smear the density gradient, resulting in an incorrect prediction of the test-filtered density-gradient magnitude,  $\rho_g(\overline{Q})$  in Eq. (28). The associated errors feed into the denominator  $\mathcal{M}_\rho$  term in the model coefficient, which manifests in the form of oscillations

of the model coefficient. The scale-similarity model, on the other hand, does not exhibit this level of scatter, and the overall trend seems to be better than the gradient model. Results using the scale-similarity model with  $C_s = 1$  and the dynamic variant were found to yield similar performance with nominal differences.

The filtered density modeled using the presumed FDF approach very closely matches the exact filtered density, with almost negligible deviation. The original formulation by Lapenna and Creta<sup>24</sup> was also compared, and the results with the model form proposed in Sec. IV E were found to be more accurate, owing to the mathematical consistency of the formulation.

The relative error in the filtered density evaluated with different models is presented as a distribution in the mixture fraction space in Fig. 6. The relative error is defined as the difference between the

modeled and exact filtered densities normalized by the exact filtered density. These are compared with the corresponding distribution for the no-model approach shown in Fig. 4(b). The error in the filtered density evaluated with the Reynolds-filtered model is roughly of the same magnitude and qualitative distribution as the no-model approach, with the difference that the error is of the opposite sign due to underprediction. This is contrary to the findings of Ribert *et al.*<sup>18</sup> for the filtered ideal gas EOS. The discrepancies are indicative of the complexities associated with the nonlinear nature of the real-fluid EOS and the important role of subgrid interactions among turbulent mixing and thermodynamics in the supercritical regime. With the dynamic gradient and scale-similarity models, the overall magnitudes of the errors are decreased. The majority of the cells display an error close to zero with a narrow error margin. The remaining scatter in the

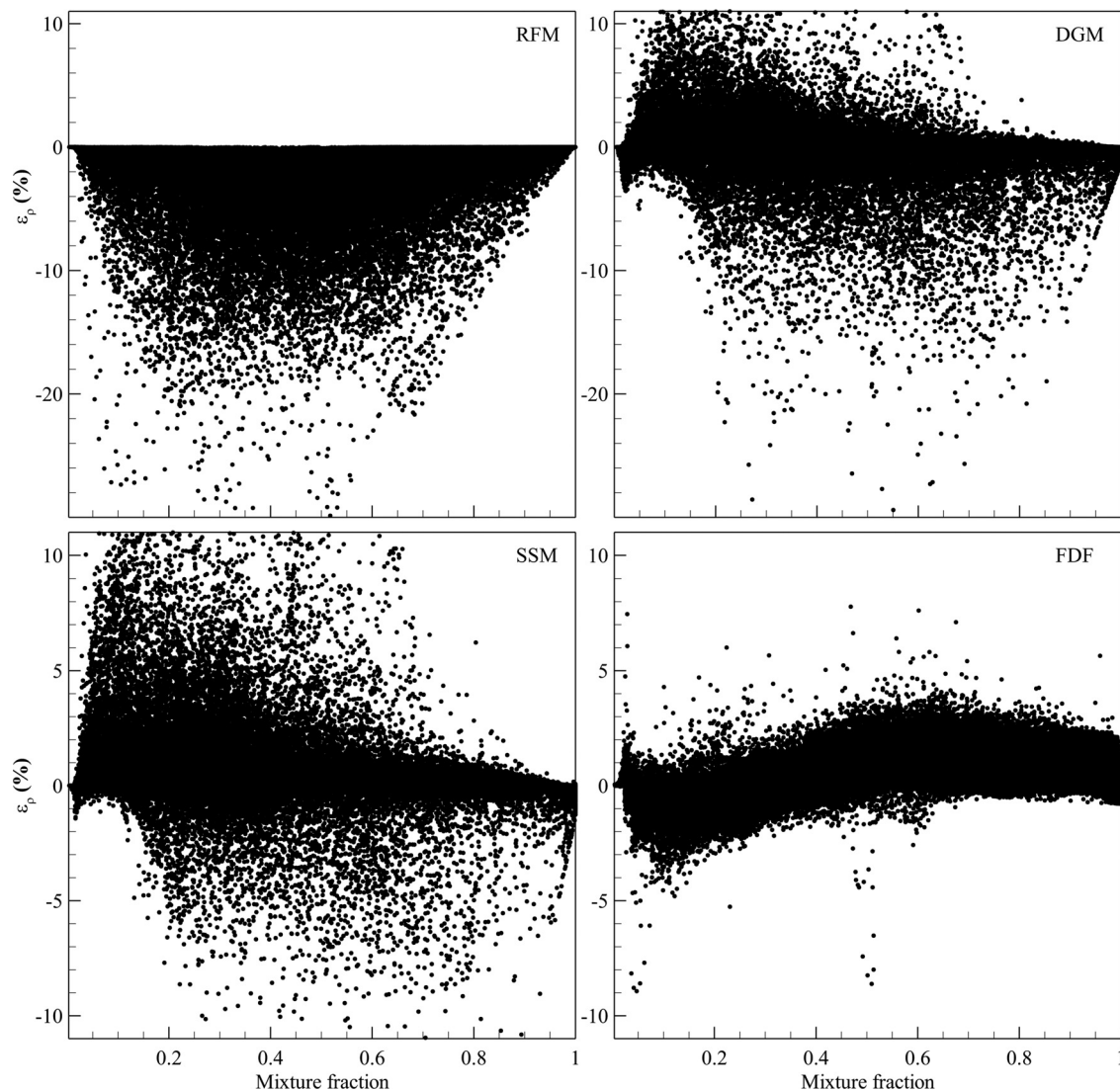


FIG. 6. Relative error in modeled filtered density as a function of mixture fraction using the different models at filter ratio  $\Delta_f = 10$ .

figures corresponds to data from cells, where the modeled filtered density is inaccurate. The subgrid density estimated by the models is sometimes overpredicted, causing the modeled filtered density to be lower than the exact value, as seen by the points with negative error. This is attributed to the oscillation of the model coefficient in those cells. The presumed FDF model shows the most improvement, with the modeling errors confined to less than 2%. The remaining errors could be a result of the numerical errors with the discrete representation of the integral, deviations of the local FDF from the presumed FDF form, or a combination.

The correlations between the exact subgrid density and the modeled subgrid density at different filter ratios are presented in Table I, and the  $L^2$  norms of the error in the modeled filtered density are presented in Table II. The correlation coefficient between the exact and modeled terms is computed using the standard relation.<sup>58</sup> For comparison, the subgrid densities for the Reynolds-filtered model and the presumed FDF model are computed as the difference between the filtered density with the no-model approach  $\rho(\tilde{Q})$  and the filtered density evaluated with the corresponding model. The error in the modeled filtered density is the difference between the exact filtered density (DNS) and the filtered density calculated using a particular model. The  $L^2$  norm of the error is computed over all the cells in the domain and normalized by the total number of cells. The modeling approaches show good improvement over the no-model approach with respect to reduction in the error norm. This performance ranking is consistent with the inferences drawn from the previous metrics. The presumed FDF approach shows the best performance in terms of the error norm and the correlation coefficient of the model prediction. The correlation coefficient of the dynamic gradient model and scale-similarity model are relatively low but are still comparable to those obtained for the conventional SGS models. With an increase in filter width, the correlations of the dynamic and scale-similarity models slightly decrease and the errors in the modeled densities increase, although the errors are still lower compared to the no-model approach. The presumed FDF model retains its accuracy even at high filter sizes both in terms of model correlation and significantly minimizing modeling errors. This observation underscores two key modeling requirements—the need for physical models to account for necessary subgrid physics, and the resolution criteria needed to ensure sufficient accuracy of the applied models.

There are advantages and limitations associated with each modeling approach proposed in this work. There remain outstanding issues with the dynamic gradient and scale-similarity modeling approaches regarding the application of test filtering in regions with strong flow gradients, and these concerns also apply to the currently used dynamic

**TABLE I.** Correlation between the exact and modeled subgrid density at different filter ratios.

Model	$\Delta_f = 5$	$\Delta_f = 10$	$\Delta_f = 20$
Reynolds-filtered	-0.94 <sup>a</sup>	-0.95 <sup>a</sup>	-0.96 <sup>a</sup>
Dynamic gradient	0.78	0.70	0.64
Scale-similarity	0.75	0.65	0.59
Presumed FDF	0.97	0.97	0.97

<sup>a</sup>Predicted values are incorrect in magnitude leading to negative correlations for the modeled densities.

**TABLE II.**  $L^2$  norms of error in the modeled filtered density at different filter ratios.

Model	$\Delta_f = 5$	$\Delta_f = 10$	$\Delta_f = 20$
No-model	11.3	76.14	316.85
Reynolds-filtered	6.76	43.39	177.81
Dynamic gradient	4.43	37.39	191.88
Scale-similarity	4.75	48.48	232.36
Presumed FDF	1.64	6.44	23.47

eddy viscosity models. However, the overall improvement in the predictions is encouraging for further refinement of these models. A consistent technique for statistical averaging of model parameters and evaluation of the test filter would be expected to further improve the model performance.

The presumed FDF model is mathematically consistent and showed the best performance among all the models investigated in this work even at higher filter ratios. A limitation of this approach, however, is that it requires additional models for estimating the subgrid-scale variances of the temperature and species fields. To evaluate these quantities, additional model transport equations must be solved.<sup>71,72</sup> Alternatively, a scale-similarity approach<sup>63</sup> or a scaling law<sup>73</sup> can be used. However, either of those approaches would be expected to introduce additional model uncertainties and errors in the framework that would be equivalent to the deficiencies in the dynamic models discussed in this study. Furthermore, the evaluation of the integrals in the model imposes additional CPU and memory costs. This is especially relevant for transcritical mixing and combustion cases, where a fine-grained density mapping in the thermodynamic state space is required to account for the strong variations in the density. This could be partially alleviated by precomputing and storing the integrals in a tabulated framework, as is performed in the use of flamelet models for combustion.<sup>74</sup>

## V. SUMMARY

The inconsistencies and errors associated with the representation of the filtered equation of state in the LES framework are investigated in the context of real-fluid mixing. The study used data from 2D DNS of a spatially evolving mixing layer consisting of gaseous methane and liquid oxygen at supercritical pressures. It is demonstrated that the direct evaluation of the filtered density (or pressure) based on the Favre-filtered thermodynamic state variables does not represent the subgrid-scale interactions between the thermodynamics and turbulent mixing, resulting in errors in the computed filtered quantity. The magnitudes of the density-weighted Favre-filtered variables are biased toward those of the denser states at the subgrid level. This results in overprediction of the filtered density computed based on these state variables for the mixing configuration considered in this study. Novel modeling approaches were proposed to account for these effects and to obtain an accurate estimate of the filtered density using the real-fluid EOS. The models were evaluated using different performance metrics to assess the accuracy in modeling the filtered density as compared to that obtained from the DNS.

The Reynolds-filtered model, in which the EOS is evaluated based on the Reynolds-filtered state variables rather than the Favre-filtered variables, does not provide any improvement over the no-

model approach. Two modeling frameworks were proposed to extend the currently used approaches to model the subgrid convective flux terms. First, a gradient model was proposed as a variant analogous to the Smagorinsky model. The formulation is based on the correlation of the subgrid density to the resolved density-gradient magnitude in the flow. To evaluate the model coefficient, a dynamic modeling procedure was formulated by applying the Germano identity, rendering the dynamic gradient model. Similarly, a scale-similarity model was proposed to directly evaluate the subgrid density. Both models were found to show improvement in representing the filtered density. Some errors persist due to unphysical variation of the model coefficient stemming from evaluation of the test-filtered quantities across sharp density-gradient regions and lack of sufficient statistical averaging. These issues are known to exist even for compressible, ideal gas flows and require further understanding. Finally, a PDF-based approach was proposed, which assumes a beta distribution form of the Favre FDF to model the subgrid-scale fluctuations of the temperature and species composition. This model showed the best correlation of the filtered density with the DNS data and the smallest modeling errors. This approach requires additional information regarding the subgrid variances of the temperature and species mass fractions, which entails supplementary models for these quantities. The model performances are evaluated at different filter ratios, highlighting the need for physically consistent modeling approaches for practical LES applications.

While the *a priori* assessments in this work are performed using 2D DNS data, the model formulations are founded on physical principles that are well established in the turbulence modeling literature and are thus expected to be valid even for realistic 3D turbulence. A key contribution of this work is understanding the role of subgrid-scale turbulence and its interactions with thermodynamics at the high Reynolds numbers and pressures that are characteristic of practical systems. Assessment of the models using 3D DNS data and *a posteriori* LES validations is warranted whenever such studies are computationally feasible.

## ACKNOWLEDGMENTS

This work was partly supported by the Air Force Office of Scientific Research (AFOSR) under grant no. FA9550-18-1-0216 and partly supported by the William R. T. Oakes Endowment and the Ralph N. Read Endowment of the Georgia Institute of Technology. The authors gratefully acknowledge support and advice from Mitat A. Birkan.

## AUTHOR DECLARATIONS

### Conflict of Interest

The authors have no conflicts of interest to disclose.

### DATA AVAILABILITY

The data that support the findings of this study are available from the corresponding author upon reasonable request.

## REFERENCES

- U. Piomelli, "Large-eddy simulation: Achievements and challenges," *Prog. Aerosp. Sci.* **35**, 335 (1999).
- C. Meneveau and J. Katz, "Scale-invariance and turbulence models for large-eddy simulation," *Annu. Rev. Fluid Mech.* **32**(1), 1–32 (2000).
- U. Piomelli, "Chapter 3: Large-eddy simulations," *Advanced Approaches in Turbulence* (Elsevier, 2021), Vol. 83.
- J. Smagorinsky, "General circulation experiments with the primitive equations I. The basic experiment," *Mon. Weather Rev.* **91**, 99 (1963).
- U. Piomelli, W. H. Cabot, P. Moin, and S. Lee, "Subgrid-scale backscatter in turbulent and transitional flows," *Phys. Fluids A* **3**, 1766 (1991).
- J. O'Brien, J. Urzay, M. Ihme, P. Moin, and A. Saghafian, "Subgrid-scale backscatter in reacting and inert supersonic hydrogen–air turbulent mixing layers," *J. Fluid Mech.* **743**, 554 (2014).
- J. Bardina, "Improved turbulence models based on large eddy simulation of homogeneous, incompressible, turbulent flows," Ph.D. thesis (Stanford University, 1983).
- M. Germano, U. Piomelli, P. Moin, and W. H. Cabot, "A dynamic subgrid-scale eddy viscosity model," *Phys. Fluids A* **3**, 1760 (1991).
- G. Erlebacher, M. Y. Hussaini, C. G. Speziale, and T. A. Zang, "Toward the large-eddy simulation of compressible turbulent flows," *J. Fluid Mech.* **238**, 155 (1992).
- P. Moin, K. Squires, W. Cabot, and S. Lee, "A dynamic subgrid-scale model for compressible turbulence and scalar transport," *Phys. Fluids A* **3**, 2746 (1991).
- C. G. Speziale, G. Erlebacher, T. A. Zang, and M. Y. Hussaini, "The subgrid-scale modeling of compressible turbulence," *Phys. Fluids* **31**, 940 (1988).
- B. Vreman, B. Geurts, and H. Kuerten, "Subgrid-modelling in LES of compressible flow," *Appl. Sci. Res.* **54**, 191 (1995).
- J. Bellan, "Theory, modeling and analysis of turbulent supercritical mixing," *Combust. Sci. Technol.* **178**, 253 (2006).
- P. E. Lapenna, "Characterization of pseudo-boiling in a transcritical nitrogen jet," *Phys. Fluids* **30**, 077106 (2018).
- T. Schmitt, L. Selle, A. Ruiz, and B. Cuenot, "Large-eddy simulation of supercritical-pressure round jets," *AIAA J.* **48**, 2133 (2010).
- M. Masquelet, S. Menon, Y. Jin, and R. Friedrich, "Simulation of unsteady combustion in a LOX-GH<sub>2</sub> fueled rocket engine," *Aerosp. Sci. Technol.* **13**, 466 (2009).
- X. Petit, G. Ribert, G. Lartigue, and P. Domingo, "Large-eddy simulation of supercritical fluid injection," *J. Supercrit. Fluids* **84**, 61 (2013).
- G. Ribert, P. Domingo, and L. Vervisch, "Analysis of sub-grid scale modeling of the ideal-gas equation of state in hydrogen–oxygen premixed flames," *Proc. Combust. Inst.* **37**, 2345 (2019).
- L. C. Selle, N. A. Okong'O, J. Bellan, and K. G. Harstad, "Modelling of subgrid-scale phenomena in supercritical transitional mixing layers: An *a priori* study," *J. Fluid Mech.* **593**, 57 (2007).
- E. S. Taskinoglu and J. Bellan, "A *posteriori* study using a DNS database describing fluid disintegration and binary-species mixing under supercritical pressure: Heptane and nitrogen," *J. Fluid Mech.* **645**, 211 (2010).
- G. Borghesi and J. Bellan, "A *priori* and *a posteriori* investigations for developing large eddy simulations of multi-species turbulent mixing under high-pressure conditions," *Phys. Fluids* **27**, 035117 (2015).
- A. Gnanaskandan and J. R. Bellan, "Large Eddy simulations of high pressure jets: Effect of subgrid scale modeling," AIAA Paper No. AIAA 2017-1105 (2017).
- G. Ribert, X. Petit, and P. Domingo, "High-pressure methane-oxygen flames. Analysis of sub-grid scale contributions in filtered equations of state," *J. Supercrit. Fluids* **121**, 78 (2017).
- P. E. Lapenna and F. Creta, "Mixing under transcritical conditions: An *a-priori* study using direct numerical simulation," *J. Supercrit. Fluids* **128**, 263 (2017).
- B. Vreman, B. Geurts, and H. Kuerten, "A priori tests of large eddy simulation of the compressible plane mixing layer," *J. Eng. Math.* **29**, 299 (1995).
- M. M. Ameen and J. Abraham, "Are '2D DNS' results of turbulent fuel/air mixing layers useful for assessing subgrid-scale models?," *Numer. Heat Transfer, Part A* **69**(1), 1–13 (2016).
- U. Unnikrishnan, H. Huo, X. Wang, and V. Yang, "Subgrid scale modeling considerations for large eddy simulation of supercritical turbulent mixing and combustion," *Phys. Fluids* **33**, 075112 (2021).
- P. E. Lapenna, G. Indelicato, R. Lamioni, and F. Creta, "Modeling the equations of state using a flamelet approach in LRE-like conditions," *Acta Astronaut.* **158**, 460 (2019).
- J. F. Ely and H. Hanley, "Prediction of transport properties. 1. Viscosity of fluids and mixtures," *Ind. Eng. Chem. Fund.* **20**, 323 (1981).

- <sup>30</sup>J. F. Ely and H. Hanley, "Prediction of transport properties. 2. Thermal conductivity of pure fluids and mixtures," *Ind. Eng. Chem. Fund.* **22**, 90 (1983).
- <sup>31</sup>J. Rowlinson and I. Watson, "The prediction of the thermodynamic properties of fluids and fluid mixtures—I. The principle of corresponding states and its extensions," *Chem. Eng. Sci.* **24**, 1565 (1969).
- <sup>32</sup>R. C. Reid, J. M. Prausnitz, and B. E. Poling, "The properties of gases and liquids," 4th ed. (McGraw-Hill, New York, New York, 1987).
- <sup>33</sup>H. Meng and V. Yang, "A unified treatment of general fluid thermodynamics and its application to a preconditioning scheme," *J. Comput. Phys.* **189**, 277 (2003).
- <sup>34</sup>J. C. Oefelein, "Advances in modeling supercritical fluid behavior and combustion in high-pressure propulsion systems," AIAA Paper No. AIAA 2019-0634 (2019).
- <sup>35</sup>D.-Y. Peng and D. B. Robinson, "A new two-constant equation of state," *Ind. Eng. Chem. Fund.* **15**, 59 (1976).
- <sup>36</sup>G. Soave, "Equilibrium constants from a modified Redlich-Kwong equation of state," *Chem. Eng. Sci.* **27**, 1197 (1972).
- <sup>37</sup>C. Pantano, R. Saurel, and T. Schmitt, "An oscillation free shock-capturing method for compressible van der Waals supercritical fluid flows," *J. Comput. Phys.* **335**, 780 (2017).
- <sup>38</sup>P. C. Ma, H. Wu, D. T. Banuti, and M. Ihme, "On the numerical behavior of diffuse-interface methods for transcritical real-fluids simulations," *Int. J. Multiphase Flow* **113**, 231 (2019).
- <sup>39</sup>H. Terashima and M. Koshi, "Approach for simulating gas-liquid-like flows under supercritical pressures using a high-order central differencing scheme," *J. Comput. Phys.* **231**, 6907 (2012).
- <sup>40</sup>H. Terashima and M. Koshi, "Strategy for simulating supercritical cryogenic jets using high-order schemes," *Comput. Fluids* **85**, 39 (2013).
- <sup>41</sup>S.-Y. Hsieh and V. Yang, "A preconditioned flux-differencing scheme for chemically reacting flows at all Mach numbers," *Int. J. Comput. Fluid Dyn.* **8**, 31 (1997).
- <sup>42</sup>N. Zong and V. Yang, "An efficient preconditioning scheme for real-fluid mixtures using primitive pressure-temperature variables," *Int. J. Comput. Fluid Dyn.* **21**, 217 (2007).
- <sup>43</sup>J. C. Oefelein and V. Yang, "Modeling high-pressure mixing and combustion processes in liquid rocket engines," *J. Propul. Power* **14**, 843 (1998).
- <sup>44</sup>N. Zong and V. Yang, "Near-field flow and flame dynamics of LOX/methane shear-coaxial injector under supercritical conditions," *Proc. Combust. Inst.* **31**, 2309 (2007).
- <sup>45</sup>X. Wang, H. Huo, U. Unnikrishnan, and V. Yang, "A systematic approach to high-fidelity modeling and efficient simulation of supercritical fluid mixing and combustion," *Combust. Flame* **195**, 203 (2018).
- <sup>46</sup>U. Piomelli, P. Moin, and J. H. Ferziger, "Model consistency in large eddy simulation of turbulent channel flows," *Phys. Fluids* **31**, 1884 (1988).
- <sup>47</sup>P. Sagaut, *Large Eddy Simulation for Incompressible Flows: An Introduction* (Springer Science & Business Media, 2006).
- <sup>48</sup>N. A. Okongo and J. Bellan, "Consistent large-eddy simulation of a temporal mixing layer laden with evaporating drops. Part 1. Direct numerical simulation, formulation and a priori analysis," *J. Fluid Mech.* **499**, 1–47 (2004).
- <sup>49</sup>Z. Ma, A. Korucu, and R. S. Miller, "A priori analysis of subgrid scale pressure and heat flux in high pressure mixing and reacting shear layers," *Combust. Theory Modell.* **19**, 807 (2015).
- <sup>50</sup>S. M. Ovais, K. A. Kemenov, and R. S. Miller, "Direct numerical simulation of supercritical oxy-methane mixing layers with CO<sub>2</sub> substituted counterparts," *Phys. Fluids* **33**, 035115 (2021).
- <sup>51</sup>V. Yang, "Modeling of supercritical vaporization, mixing, and combustion processes in liquid-fueled propulsion systems," *Proc. Combust. Inst.* **28**, 925 (2000).
- <sup>52</sup>N. Zong, H. Meng, S.-Y. Hsieh, and V. Yang, "A numerical study of cryogenic fluid injection and mixing under supercritical conditions," *Phys. Fluids* **16**, 4248 (2004).
- <sup>53</sup>R. C. Swanson and E. Turkel, "On central-difference and upwind schemes," *J. Comput. Phys.* **101**, 292 (1992).
- <sup>54</sup>M. S. Graboski and T. E. Daubert, "A modified Soave equation of state for phase equilibrium calculations. 2. Systems containing CO<sub>2</sub>, H<sub>2</sub>S, N<sub>2</sub>, and CO," *Ind. Eng. Chem. Proc. Des. Dev.* **17**, 448 (1978).
- <sup>55</sup>D. T. Banuti, "Crossing the widom-line—Supercritical pseudo-boiling," *J. Supercrit. Fluids* **98**, 12 (2015).
- <sup>56</sup>R. A. Clark, J. H. Ferziger, and W. C. Reynolds, "Evaluation of subgrid-scale models using an accurately simulated turbulent flow," *J. Fluid Mech.* **91**, 1–16 (1979).
- <sup>57</sup>U. Unnikrishnan, X. Wang, S. Yang, and V. Yang, "Subgrid scale modeling of the equation of state for turbulent flows under supercritical conditions," AIAA Paper No. AIAA 2017-4855 (2017).
- <sup>58</sup>M. P. Martin, U. Piomelli, and G. V. Candler, "Subgrid-scale models for compressible large-eddy simulations," *Theor. Comput. Fluid Dyn.* **13**, 361 (2000); available at <https://link.springer.com/article/10.1007/PL00020896>
- <sup>59</sup>D. K. Lilly, "A proposed modification of the Germano subgrid-scale closure method," *Phys. Fluids A* **4**, 633 (1992).
- <sup>60</sup>S. Ghosal, T. S. Lund, P. Moin, and K. Akselvoll, "A dynamic localization model for large-eddy simulation of turbulent flows," *J. Fluid Mech.* **286**, 229 (1995).
- <sup>61</sup>Y. Zang, R. L. Street, and J. R. Koseff, "A dynamic mixed subgrid-scale model and its application to turbulent recirculating flows," *Phys. Fluids A* **5**, 3186 (1993).
- <sup>62</sup>S. Liu, C. Meneveau, and J. Katz, "On the properties of similarity subgrid-scale models as deduced from measurements in a turbulent jet," *J. Fluid Mech.* **275**, 83 (1994).
- <sup>63</sup>A. W. Cook and J. J. Riley, "A subgrid model for equilibrium chemistry in turbulent flows," *Phys. Fluids* **6**, 2868 (1994).
- <sup>64</sup>S. B. Pope, *Turbulent Flows* (Cambridge University Press, 2000).
- <sup>65</sup>P. J. Colucci, F. A. Jaber, P. Givi, and S. B. Pope, "Filtered density function for large eddy simulation of turbulent reacting flows," *Phys. Fluids* **10**, 499 (1998).
- <sup>66</sup>P. Givi, "Filtered density function for subgrid scale modeling of turbulent combustion," *AIAA J.* **44**, 16 (2006).
- <sup>67</sup>C. Wall, B. J. Boersma, and P. Moin, "An evaluation of the assumed beta probability density function subgrid-scale model for large eddy simulation of non-premixed, turbulent combustion with heat release," *Phys. Fluids* **12**, 2522 (2000).
- <sup>68</sup>F. A. Jaber, P. J. Colucci, S. James, P. Givi, and S. B. Pope, "Filtered mass density function for large-eddy simulation of turbulent reacting flows," *J. Fluid Mech.* **401**, 85 (1999).
- <sup>69</sup>P. Sagaut and M. Germano, "On the filtering paradigm for LES of flows with discontinuities," *J. Turbul.* **6**, N23 (2005).
- <sup>70</sup>D. V. Kotov, H. C. Yee, A. A. Wray, A. Hadjadj, and B. Sjögren, "High order numerical methods for the dynamic SGS model of turbulent flows with shocks," *Commun. Comput. Phys.* **19**, 273 (2016).
- <sup>71</sup>C. Pera, J. Réveillon, L. Vervisch, and P. Domingo, "Modeling subgrid scale mixture fraction variance in LES of evaporating spray," *Combust. Flame* **146**, 635 (2006).
- <sup>72</sup>K. A. Kemenov, H. Wang, and S. B. Pope, "Modelling effects of subgrid-scale mixture fraction variance in LES of a piloted diffusion flame," *Combust. Theory Modell.* **16**, 611 (2012).
- <sup>73</sup>C. D. Pierce and P. Moin, "A dynamic model for subgrid-scale variance and dissipation rate of a conserved scalar," *Phys. Fluids* **10**, 3041 (1998).
- <sup>74</sup>P. Kundu, M. M. Ameen, C. Xu, U. Unnikrishnan, T. Lu, and S. Som, "implementation of detailed chemistry mechanisms in engine simulations," *J. Eng. Gas Turbines Power* **141**, 0111026 (2019).